Journal of Medicinal Chemistry

Article

pubs.acs.org/jmc

G-Protein-Coupled Bile Acid Receptor 1 (GPBAR1, TGR5) Agonists Reduce the Production of Proinflammatory Cytokines and Stabilize the Alternative Macrophage Phenotype

Klemens Högenauer,*[,†] Luca Arista,[†] Niko Schmiedeberg,[†] Gudrun Werner,[‡] Herbert Jaksche,[‡] Rochdi Bouhelal,[§] Deborah G. Nguyen,[∥,⊥] B. Ganesh Bhat,[∥] Layla Raad,[‡] Celine Rauld,[‡] and José M. Carballido[‡]

[†]Global Discovery Chemistry, [‡]Autoimmunity, Transplantation and Inflammation, and [§]Center for Proteomic Chemistry, Novartis Institutes for BioMedical Research, Novartis Campus, CH-4056 Basel, Switzerland

[∥]Genomics Institute of the Novartis Research Foundation, 10675 John Jay Hopkins Drive, San Diego, California 92121, United States

Supporting Information

ABSTRACT: GPBAR1 (also known as TGR5) is a G-protein-coupled receptor (GPCR) that triggers intracellular signals upon ligation by various bile acids. The receptor has been studied mainly for its function in energy expenditure and glucose homeostasis, and there is little information on the role of GPBAR1 in the context of inflammation. After a high-throughput screening campaign, we identified isonicotinamides exemplified by compound **3** as nonsteroidal GPBAR1 agonists. We optimized this series to potent derivatives that are active on both human and murine GPBAR1. These agonists inhibited the secretion of the proinflammatory cytokines TNF-α and IL-12 but not the antiinflammatory IL-10 in primary human monocytes. These effects translate in vivo, as compound **15** inhibits LPS induced TNF-α and IL-12 release in mice. The response was GPBAR1 dependent, as demonstrated using knockout mice. Furthermore, agonism of GPBAR1 stabilized the phenotype of the alternative, noninflammatory, M2-like type cells during differentiation of monocytes into macrophages. Overall, our results illustrate an important regulatory role for GPBAR1 agonists as controllers of inflammation.

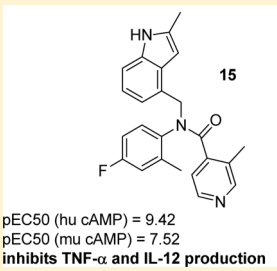

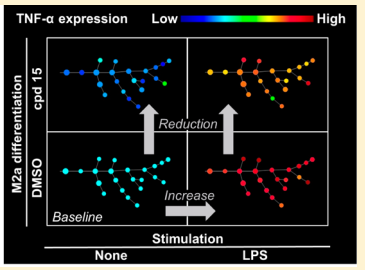

INTRODUCTION

Since the discovery of the G-protein-coupled bile acid receptor 1 GPBAR1 (also known as TGR5),[1] there has been an increased interest to pharmacologically modulate this target. GPBAR1 was found to be involved in lipid and glucose metabolism as well as energy expenditure, and in this context, receptor agonists are being pursued by various pharmaceutical companies to offer treatment options for conditions such as obesity, hypercholesterolemia, hypertriglyceridemia, and non-alcoholic steatohepatitis.[2] Most importantly, the finding that GPBAR1 agonism induces the secretion of clinically relevant glucagon-like peptide 1 (GLP-1) raised expectations of an alternative therapeutic mechanism for the treatment of type 2 diabetes mellitus[3] and triggered extensive research efforts.[4−17]

The potential of this receptor in immunology and inflammation was outlined when bile acids (BAs), acting as receptor agonists, showed reduced lipopolysaccharide (LPS) induced release of the proinflammatory cytokines TNF-α, IL-1, IL-6, and IL-8 in rabbit alveolar macrophages.[1] For a long period, the link to immunology was the subject of very few follow-up studies.[18−20] Recently, it was shown that bile acids drive dendritic cell (DC) differentiation from monocytes toward a IL-12 hypo-producing phenotype via the GPBAR1 pathway.[21] Studies in mice suggest that GPBAR1 agonism suppresses cytokine secretion via impaired NF-κB signaling.[22] In addition, a study in human macrophages reported that bile acids leave the production of antiinflammatory cytokine IL-10 unaffected and only inhibit the secretion of proinflammatory cytokines TNF-α, IL-6 and IL-12p40.[23] This observation indicates that GPBAR1 activation does not completely block cytokine expression but rather shifts the pattern toward that of an antiinflammatory macrophage.[24]

We became interested in GPBAR1 in the course of our search for selective immunomodulatory principles capable of rebalancing immune inflammatory responses without inducing systemic immunosuppressive effects. The goal of our drug discovery program was to identify rodent cross-reactive compounds suited to advance target validation and development of orally efficacious antiinflammatory therapeutics.

RESULTS AND DISCUSSION

Target Biology and Hit-Finding. We tested various conjugated and unconjugated bile acids in a Ca^{2+}-mobilization assay in Jurkat cells stably expressing human (hu) or murine (mu) GPBAR1 after retroviral transduction. Although GPBAR1

Received: July 15, 2014

   dx.doi.org/10.1021/jm501052c | J. Med. Chem. XXXX, XXX, XXX−XXX

is coupled to adenylyl cyclase through the $G_{\alpha s}$ GTP binding protein, it proved possible to monitor its activation through endogenous $G_{\alpha 15}$ and $G_{\alpha 16}$ promiscuous protein in Jurkat cells. This association enables coupling of the vast majority of $G_{\alpha s}$ and $G_{\alpha i}$ coupled receptors to PLC_{β} and Ca^{2+}-mobilization following receptor activation. We found that taurolitocholic acid (TLCA, **1**, Figure 1) was one of the most potent and cross-

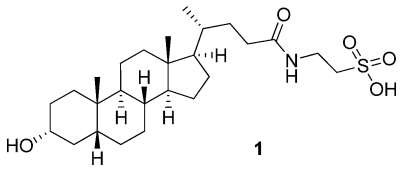

1

Figure 1. Structure of taurolitocholic acid (TLCA, **1**).

reactive bile acids (hu pEC_{50} = 7.27, mu pEC_{50} = 6.54) with comparable activity on cAMP stimulation (Table 1). TLCA also inhibited the production of TNF-α and IL-12 in isolated human monocytes (Table 2). Elevations in cellular cAMP have been shown to inhibit production of TNF-α from myeloid cells, further supporting a link between Gs-coupled GPBAR1 activation and modulation of inflammatory cytokine production.[25,26] Similar to reported observations with macrophages,[23] secretion of the antiinflammatory cytokine IL-10 remained at DMSO control levels. Selective inhibition of proinflammatory cytokines has been suggested to be a major driver for monocyte differentiation toward the M2 macrophage phenotype which is associated with resolution of inflammatory processes.[27] This offers new therapeutic opportunities for diseases characterized by an overshooting Th1/Th17 cell component (such as multiple sclerosis, psoriasis, or type 1 diabetes).

Table 1. cAMP and Ca^{2+}-Mobilization Assay Data Directed the Optimization of the Carboxylic Acid Fragment of Carboxamides

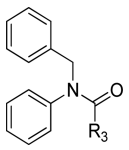

	R_3	hu GPBAR1 pEC_{50} (SD)[a]		mu GPBAR1 pEC_{50} (SD)[a]	
		cAMP	Ca^{2+}-flux	cAMP	Ca^{2+}-flux
1	n.a.	7.70 (0.29)	7.27 (0.35)	6.64 (0.24)	6.54 (0.18)
2		7.32 (0.38)	6.91 (0.44)	5.39 (0.16)	<4.62
3		6.84 (0.66)	6.32 (0.35)	5.36 5.25	<4.62
4		7.19 6.58	5.79 (0.28)	n.d.	<4.62
5		7.95 (0.20)	7.43 (0.11)	5.99 (0.25)	5.10 (0.17)
6		<4.70	<4.62	<4.70	<4.62
7		7.49 7.52	6.38 6.48	<4.70	<4.62
8		8.55 8.29	7.43 (0.11)	5.82 5.36	5.14 (0.19)

[a] pEC_{50} values are the mean of at least three runs performed in four replicates with standard deviation in parentheses. For n = 2, individual values are reported.

We screened the Novartis compound archive in order to find nonsteroidal GPBAR1 agonists in a Ca^{2+}-mobilization assay format. We identified a number of chemically diverse hits that specifically activate GPBAR1, as they only showed significant induction of Ca^{2+}-mobilization in cells expressing GPBAR1. Active hits (total number 1229) were also tested in an orthogonal assay format (cAMP production), and compounds that were inactive in this assay were not further pursued. For compounds that were active in both assays (in total 384), a reasonable correlation (R^2 = 0.46) between EC_{50} values was observed (Figure 2). Differences are explained by GPBAR1 kinetics, as different incubation times were employed in the two assays. To ensure both proximal and downstream functional response of our agonists, we decided to run both assays in parallel during our optimization program. After this hit validation, we became interested in a cluster around the hit compounds **2** and **3** (Table 1). These comparatively small derivatives showed considerable activity on the human GPBAR1 receptor. The moderate lipophilicity of these compounds (HT-logP = 3.4 for compound **2** and HT-logP = 3.2 for compound **3**)[28] made them attractive starting points for lead optimization (hu cAMP LipE = 3.9 for compound **2** and hu cAMP LipE = 3.6 for compound **3**, based on measured log P).[29]

Synthesis. Derivatives of isoxazole **2** and isonicotinamide **3** were assembled in a straightforward manner forming the amide bond in the final step. Noncommercially available secondary amines were prepared using reductive amination. Unexpectedly, the amide bond formation was quite problematic, especially when combinations of hindered carboxylic acids and electron deficient aniline building blocks were used. Many standard coupling conditions tested (DCC, EDC, HOBt, PyBOP, HATU) were either low-yielding or failed to give any product. We then switched to preparing the carboxylic acid chlorides in situ from the carboxylic acids. Either 1-chloro-*N*,*N*,2-trimethylprop-1-en-1-amine[30] or $POCl_3$/pyridine gave acceptable yields for this transformation. Scheme 1 shows the synthesis of indole **15** as a representative example.

In Vitro SAR. Both compounds **2** and **3** were inactive in the murine version of the Ca^{2+}-mobilization assay and only showed high micromolar activity in the murine cAMP assay. As one of our goals was to show pharmacological effects in a rodent model, our optimization efforts were geared toward establishing cross-reactivity for the mouse receptor. When probing the SAR of the carboxylic acid fragment (Table 1), we found that 3-methylpyridine **5** combined a more than 10-fold potency increase on the human receptor with at least measurable activity on the mouse ortholog. Lipophilicity for this derivative is still in a reasonable range (HT-logP = 3.2), resulting in an overall

dx.doi.org/10.1021/jm501052c | J. Med. Chem. XXXX, XXX, XXX−XXX

Table 2. cAMP, Ca^{2+}-Mobilization and Primary Cell Assay Data Guiding the Optimization of Isonicotinamides

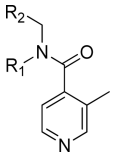

	R_1	R_2	hu GPBAR1 pEC_{50}[a]		mu GPBAR1 pEC_{50}[a]		hu monocytes pIC_{50}[a]		
			cAMP	Ca^{2+}-flux	cAMP	Ca^{2+}-flux	TNF-α	IL-12p40	IL-10
1	n.a.	n.a.	7.70 (0.29)	7.27 (0.35)	6.64 (0.24)	6.54 (0.18)	5.21 (0.09)	5.16 (0.11)	<5
9			6.87	6.67	n.d.	<4.62	n.d.	n.d.	n.d.
10			7.13 6.89	6.06 (0.20)	5.25 4.96	<4.62	<5.00	<5.00	<5
11			7.61 7.01	6.76 (0.30)	5.60 (0.18)	<4.62	n.d.	n.d.	n.d.
12			7.88	>8.12	6.66 6.42	5.81 (0.24)	n.d.	n.d.	n.d.
13			9.51 9.49	>8.12	7.16 7.16	6.57 (0.43)	7.28 (0.56)	7.14 (0.57)	<5
14			9.52 9.20	>8.12	7.69 (0.12)	6.06 (0.64)	7.24 (0.38)	7.28 (0.31)	<5
15			9.42 (0.12)	>8.12	7.52 (0.19)	7.43 (0.24)	7.01 6.93	7.17 7.08	<5

[a] pEC_{50} and pIC_{50} values are the mean of at least three runs performed in four replicates with standard deviation in parentheses. For $n = 1$ or $n = 2$, individual values are reported.

improved LipE of 4.8. The position of the methyl group is important, as shifting it into the 2-position of the pyridine resulted in a significant activity drop in all assays (2-methylpyridine **4**). Altering the position of the nitrogen as in pyridine isomer **6** led to complete activity loss. Adding another nitrogen (pyridazine **7**) was detrimental for mouse cross-reactivity. We also tested a number of five-membered heterocyclic carboxylic acid fragments. Whereas dimethylisoxazole **2** was selective for human GPBAR1, methylimidazole **8** showed comparable cross-reactivity potential to 3-methylpyridine **5**.

Next, we turned to investigate the substitution pattern on the amine moiety (Table 2). Since neither one-carbon homologues of benzylanilide **5** (amides **9** and **10**) nor replacements of the benzyl group by alkyl substituents (e.g., isobutyl derivative **11**) led to an improved murine assay activity, we decided to keep the *N*-benzylaniline framework and focus on optimization of the substitution pattern. Considerable activity gain in the mouse assays could be achieved by introducing ortho-substituents on the aromatic ring of the benzylamine. The 2-methoxybenzyl derivative **12** showed a ∼4-fold activity gain on murine GPBAR1 compared to the unsubstituted benzylanilide **5**. When we combined this modification with appropriate substitution on the anilinic phenyl group, we observed a significant activity increase on both human and mouse receptors. Ortho-trifluoromethoxyanilide **13** and dichloroanilide **14** are subnanomolar human GPBAR1 agonists with considerable potency in the mouse cAMP assay. These derivatives were also tested for their ability to inhibit LPS induced cytokine release in primary human monocytes. Indeed, both carboxamides **13** and **14** potently inhibit the secretion of TNF-α and the p40 subunit of IL-12 with in vitro activities 100-fold higher than TLCA. Similar to our observations with TLCA, IL-10 secretion remains unaffected, highlighting that GPBAR1

dx.doi.org/10.1021/jm501052c | J. Med. Chem. XXXX, XXX, XXX−XXX

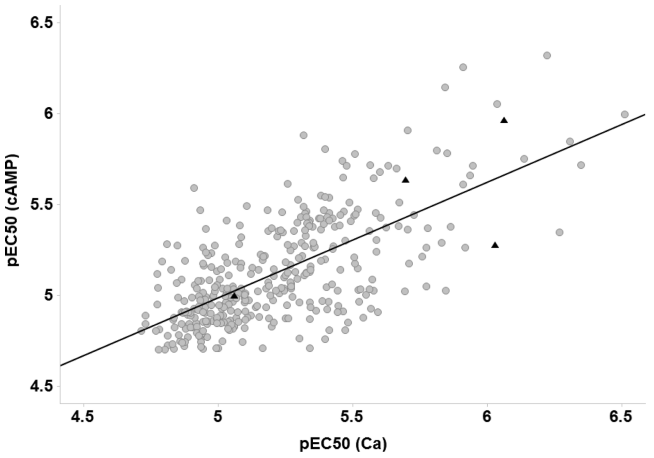

Figure 2. Out of a total number of 1229 hits in the hu GPBAR1 Ca^{2+}-mobilization assay, 384 hits (shown as dots and triangles) were also active in the hu cAMP assay. pEC_{50} values were determined as $n = 1$ in a miniaturized version of the assays. Cluster representatives described in the text are indicated as black triangles. The black line represents least-squares regression line ($R^2 = 0.46$).

agonists selectively inhibit proinflammatory cytokine production. For our planned in vivo model in mice, we continued to search for compounds with an improved Ca^{2+}-mobilization activity on murine cells without compromising activity on human primary cells. We identified indole **15** as a compound with an attractive cellular profile (murine Ca^{2+}-flux EC_{50} = 7.43). Compared to the initial hit compound **3**, indole **15** is still reasonably small and displays moderate lipophilicity (HT-logP = 3.8),[28] illustrating that we were able to optimize potency in a lipophilicity efficient manner (hu cAMP LipE = 5.6). The activity in human primary cells of indole **15** was also compared to piperidine-3-carboxamide **16** (Figure 3), a recently published potent GPBAR1 agonist from a different structural class (chronologically, that series was discovered after the carboxamides described in the current manuscript).[17] In human peripheral blood mononuclear cells (PBMCs),[17] secretion of the key cytokine TNF-α was inhibited to a similar degree by both compounds (Table 3). In addition neither compound showed an effect on the antiinflammatory cytokine IL-10. Presumably because of its high unspecific binding, TLCA **1** did not show any inhibition up to 10 μM. In a safety panel screen of 64 off-target assays (for a full list, see Supporting Information), indole **15** showed only moderate inhibition of human opiate κ (IC_{50} = 1.3 μM) and opiate μ receptors (IC_{50} = 5.9 μM) while all other targets tested displayed IC_{50} values of >10 μM. In addition, indole **15** did not show any activity on FXR, a nuclear hormone receptor responsive to bile acids (in a cellular Gal4 reporter gene assay, run in both agonist and

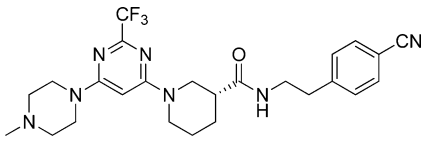

16

Figure 3. Structure of the recently disclosed GPBAR-1 agonist piperidinecarboxamide **16**.[17]

Table 3. Comparison of Cytokine Inhibition Profile in Human PBMCs for Key Compounds

		hu PBMCs pIC_{50} [a]	
compd	hu GPBAR1 pEC_{50},[a] cAMP	TNF-α	IL-10
1	7.70 (0.29)	<5.00	<5.00
15	9.42 (0.12)	6.84	<5.00
16	8.52 (0.48)	7.04	<5.00

[a] pEC_{50} and pIC_{50} values are the mean of at least three runs performed in four replicates with standard deviation in parentheses. For $n = 1$, individual values are reported.

antagonist settings, the compound did not generate a response up to a concentration of 10 μM).

Role of GPBAR1 on Macrophage Differentiation. Because GPBAR1 agonists effectively suppress proinflammatory cytokine production by macrophages, we assessed whether their presence during monocyte differentiation would also affect lineage commitment toward proinflammatory (M1) or proresolving (M2) macrophage types. The experiment involved the differentiation of human primary monocytes in the presence of macrophage colony-stimulating factor (M-CSF) either alone or together with IFN-γ or IL-4 to drive neutral, M1, or M2 differentiation, respectively.[27] Surface and cytokine analysis was performed using a mass cytometer (CyTOF), which assesses the simultaneous presence of large arrays of antibodies, conjugated to monoisotopic lanthanides, by monitoring the time-of-flight of the different metal tags.[31] Figure 4 shows that cell populations separated into three distinct clusters after a 6-day differentiation period, based on a spanning-tree progression analysis of density-normalized events (SPADE)[31] performed using CyToBank software. GPBAR1 agonist indole **15** did not change the fate of macrophage differentiation imposed by the cytokine cocktails. Particularly, indole **15** did not alter the expression of surface markers such as CD38 or CD200R and CD206, which are classically associated with M1 or M2 differentiation, respectively (Supporting Information Figure 1). If at all, GPBAR1 agonism enhanced the expression of overall co-stimulatory molecules on both M1 and M2 cell populations and potentiated the lineage associated markers on both M1 and M2 cell types (Supporting Information Figure 1), suggesting that the presence of

Scheme 1. Reductive Amination/Amide Bond Formation Sequence Exemplified for the Synthesis of Indole 15

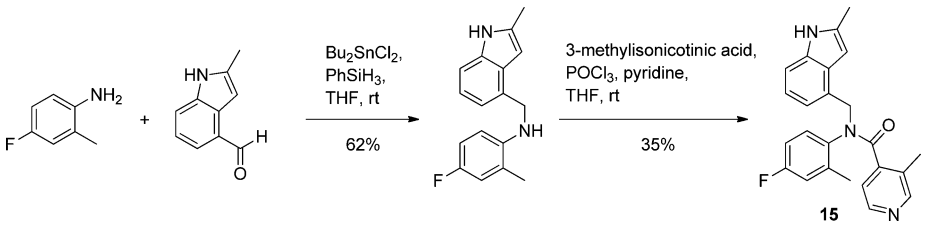

dx.doi.org/10.1021/jm501052c | J. Med. Chem. XXXX, XXX, XXX–XXX

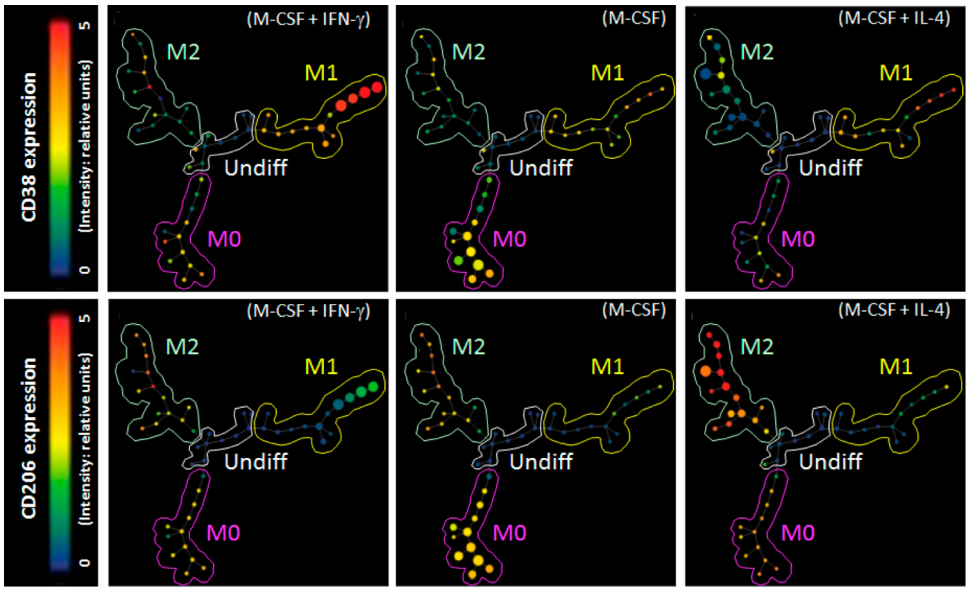

Figure 4. SPADE analysis on all different data files, including macrophages differentiated with the different combinations of cytokines in the presence or absence of indole **15** (3 μM), generates three distinct cell clusters, labeled M0, M1, and M2. The intensity of expression of representative M1 and M2 differentiation markers CD38 and CD206, respectively, on the different (M0, M1, and M2) clusters of macrophage populations differentiated with the indicated cytokine cocktail in the absence of GPBAR1 agonists is indicated as a heat map. Each sphere represents a potential cell subpopulation, and its size is proportional to the number of cells contained in such subgroup. Cytokine cocktails forced >85% of the differentiating cells to group in one of the three major clusters.

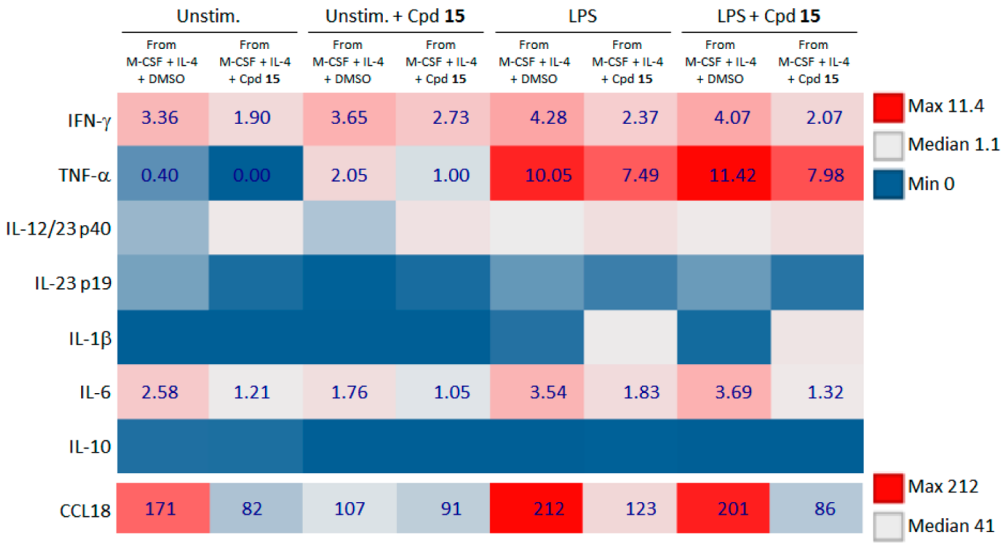

Figure 5. Intracellular cytokine production by resting and LPS-stimulated human M2 macrophages. The presence of indole **15** (3 μM) during M2 cell differentiation primes macrophages for sustained reduction of inflammatory cytokine/chemokine production. Shown are results of intracellular analysis of M2 cells gated on single, living, CD45 positive cells, expressing CD14 and CD64 markers, which were differentiated for 7 days with M-CSF and IL-4 in the absence or presence of indole **15** (3 μM). Cells were left unstimulated or were activated with LPS for an additional 24 h in the presence or absence of indole **15** (3 μM). Expression is visualized as a relative intensity heat map of independent CyTOF dual counts per second. Values for the proinflammatory cytokines IFN-γ, TNF-α, and IL-6 and chemokine CCL18 are indicated inside the cells to enhance data visualization. The CCL18 heat map is presented separately from the other cytokines because of its higher relative expression.

polarizing cytokines is determinant over GPBAR1 signaling in inducing macrophage differentiation. M2 cells, previously differentiated in the presence or absence of GPBAR1 agonist, were harvested and recultured without differentiating factors for an additional 24 h in control medium or medium containing LPS in the presence or absence of indole **15**. In the absence of any polarizing cytokine, M2 cells maintained their overall M2 surface phenotype. However, the cells differentiated in the presence of the GPBAR1 agonist maintained a higher expression of co-stimulatory molecules (such as CD11c, CD40, CD64, and HLA-DR) as well as higher expression of the M2 lineage markers (CD200R and CD206) than their counterparts derived from cultures devoid of indole **15** during differentiation (Supporting Information Figure 2). These effects were specific, since other low abundance M2 cell surface molecules, such as CD38, were not increased. Cytokine production was also simultaneously assessed at the single level to determine whether chronic or acute exposure to

dx.doi.org/10.1021/jm501052c | J. Med. Chem. XXXX, XXX, XXX−XXX

GPBAR1 agonism would change the frequencies of cytokine producing cells. The direct effects of indole **15** on the frequency of cytokine producing cells were marginal. In contrast, both overall baseline and LPS induced proinflammatory factor production were consistently lower in the cultures exposed to indole **15** during the 6-day differentiation period (Figure 5, Supporting Information Figures 3 and 4). In summary, these results suggest that GPBAR1 agonism not only suppresses the overall production of proinflammatory cytokines but also contributes to the stabilization of the antiinflammatory M2 cell phenotype (as observed by the larger frequency of cells displaying M2 surface markers and reduced inflammatory factor production).

In Vivo Characterization. During our optimization efforts, we determined high in vitro clearance in microsomal preparations (human and rodent) throughout the series. This metabolic instability was log *P* independent and likely caused by the presence of a number of oxidizable functionalities and the potential for metabolic switching. As indole **15** also showed prominent in vitro metabolism ($t_{1/2}$ in mouse liver microsomes of 2 min),[32] we did not expect prolonged exposure in vivo. Indeed, in vivo clearance in mice was high and terminal half-life was short, yet the compound showed rapid absorption (early T_{max}) and a moderate oral bioavailability (Table 4). In order to ensure adequate exposure, pharmacokinetic experiments were also conducted at high dose. After some experimentation, we found that the use of a microemulsion (45% Cremophor RH40, 36% corn oil glycerides, 9% propylene glycerol, 10% ethanol)[33] resulted in both sufficient exposure and low inter-animal variability. By use of this formulation, both total and unbound mouse plasma levels (mouse PPB = 98%, determined by rapid equilibrium dialysis) exceed the EC_{50} in the murine Ca^{2+}-mobilization assay in the first 5 h after dosing at a po dose of 50 mg/kg (Figure 8). As in the acute model of LPS induced cytokine release the terminal readout is taken 3.5 h after dosing, these parameters were considered sufficiently supportive for in vivo efficacy evaluation of indole **15**. It should be noted that the previously mentioned series around piperidine-3-carboxamide **16**, which combines a comparable cellular profile with better pharmacokinetics, had not been discovered at that time.

Vehicle treatment of both WT and KO animals resulted in similar levels of TNF-α production (Figure 6). Indole **15** (50 mg/kg po) inhibited LPS induced TNF-α production in WT animals from a mean of 1554 pg/mL (95% CI = 1955−1153 pg/mL) to a mean of 578 pg/mL (95% CI = 965−191 pg/mL, p = 0.005). The effect was modest compared to the antiinflammatory glucocorticoid dexamethasone (5 mg/kg).[34] In KO mice, treatment with indole **15** had no effect on TNF-α levels, confirming that the effect observed in WT mice was indeed GPBAR1 dependent. Figure 7 illustrates that indole **15** markedly inhibits LPS induced IL-12 production from a mean of 456 pg/mL (95% CI = 523−389 pg/mL) to a mean of 205 pg/mL (95% CI = 262−148 pg/mL, $p = 7 \times 10^{-5}$); the reduction is similar to dexamethasone treatment. The GPBAR1 dependence of this effect is only observed as a trend, most probably due to the low IL-12 production by the vehicle treated KO group. Serum levels of IL-10, IL-1β, IL-6, mKC, and IFN-γ were below detection limit (data not shown).

Table 4. Mouse PK Parameters[a] for Indole 15

route (dose in mg·kg^{-1})	iv (2.5)	po (10)
CL [mL·min^{-1}·kg^{-1}]	146	
V_{SS} [L·kg^{-1}]	3.0	
$t_{1/2}$ term. [h]	0.64	
AUC dn[b] [μg·min·mL^{-1}]	6.9	2.8
abs oral BAV [%]		41
C_{max} dn[b] [nM]		95
T_{max} [h]		0.5

[a]Male C57BL/6 mice; each time point from three single sacrificed animals. iv: bolus administration of 2.5 mg·kg^{-1}, dissolved in *N*-methylpyrrolidone/mouse plasma = 10:90, v/v, sampling 5, 30, 60, 120, 240, 480, 1440 min after administration. po: 10 mg·kg^{-1}, suspended in 0.5% carboxymethyl cellulose and 0.5% polysorbate 80 in water, sampling 15, 30, 60, 120, 240, 480, 1440 min after administration. [b]dn = dose normalized.

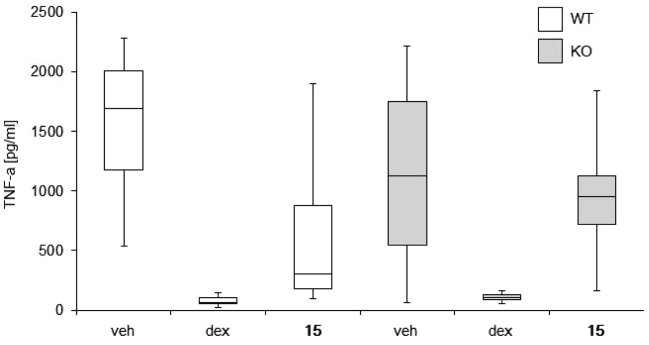

Figure 6. Indole **15** (50 mg/kg) inhibits LPS induced TNF-α production in WT but not in GPBAR1 KO mice. Box plot (generated using a Microsoft Excel 2010 template, with bottom and top of the box showing first and third quartiles, inside band showing median, whiskers representing minimum and maximum of all data; outliers significantly outside 1.5 times interquartile range were removed) shows the results from a minimum of n = 8 individual mice. veh = vehicle control, dex = dexamethasone (5 mg/kg).

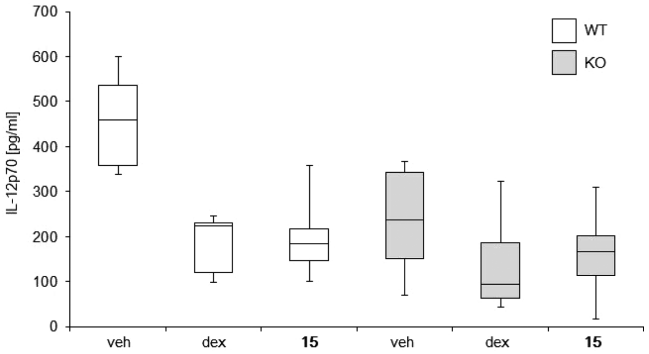

Figure 7. Indole **15** (50 mg/kg) inhibits LPS induced IL-12p70 production in WT but not in GPBAR1 KO mice. Box plot (description see Figure 6) shows results from a minimum of n = 8 individual mice.

SUMMARY AND CONCLUSIONS

We have developed a mouse cross-reactive series of GPBAR1 agonists with high potency in both cAMP production and Ca^{2+}-mobilization assays. In agreement with early findings using bile acids as tools, optimized compounds such as indole **15** are potent inhibitors of the proinflammatory cytokines TNF-α and IL-12 in isolated human monocytes, whereas levels of the antiinflammatory cytokine IL-10 remain unaffected. Using indole **15**, we could demonstrate the contribution of GPBAR1 agonism to the overall differentiation and stability

dx.doi.org/10.1021/jm501052c | J. Med. Chem. XXXX, XXX, XXX−XXX

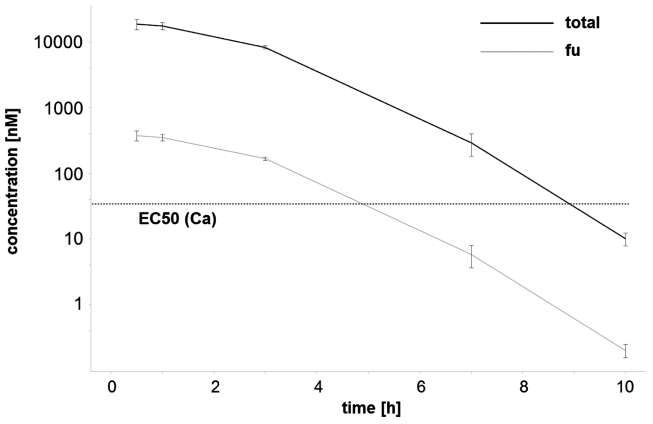

Figure 8. Total and unbound plasma concentration of indole **15** in Balb/C mice (50 mg/kg po, n = 3, same vehicle as for the in vivo experiment depicted in Figures 6 and 7, mouse PPB = 98%). The dotted line indicates the murine Ca^{2+}-mobilization EC_{50}. Error bars show standard deviation.

of the antiinflammatory M2 cell phenotype. Macrophages are very plastic cells, and they can differentiate and redifferentiate back and forward into M1 and M2 cell subsets in vitro.[27] Secondary bile acids are generated in the intestinal tract from primary bile acids with the help of *Clostidrium* bacteria. In view of the prominent role of the microbiome controlling immune regulation, it is tempting to speculate that GPBAR1 agonists mimic one of the most ancient immunoregulatory mechanisms provided by evolution to sustain homeostatic antiinflammatory cell differentiation.

Although indole **15** was shown to exhibit a short half-life in mice, the achieved exposure was sufficient to demonstrate in vivo activity in an acute model of LPS-induced cytokine release. This compound reduced TNF-α and IL-12 production at 50 mg/kg in vivo, a dose where both total and unbound compound concentration exceeded EC_{50} levels in the murine Ca^{2+}-mobilization assay for this compound over the whole time of the experiment. Compared to the broad immunosuppressant dexamethasone, the effects on TNF-α and IL-12 production were moderate, yet selective for proinflammatory cytokines. Indole **15** had no effect on cytokine levels of GPBAR1 KO mice, thereby confirming GPBAR1 dependency for the observed effects. Overall, we could confirm our initial hypothesis that GPBAR1 is an appropriate target for the treatment of inflammatory diseases. However, the modest in vivo effects of indole **15** at comparatively high doses as well as the significant ADME hurdles that needed to be overcome led us to discontinue our efforts in this compound series.

EXPERIMENTAL SECTION

Chemistry. Unless otherwise stated, all reagents and solvents were purchased from commercial suppliers and used without further purification. TLCA (**1**) was purchased from Sigma (catalog no. T-7515). ^{1}H NMR spectra were recorded on a Bruker 400 MHz or a Bruker 600 MHz NMR spectrometer. Chemical shifts are reported in parts per million (ppm) relative to an internal solvent reference. Recorded peaks are listed in the order multiplicity (s, singlet; d, doublet; t, triplet; q, quartet; qt, quintet; m, multiplet; br, broad), coupling constants, and number of protons. Final compounds were purified to ≥95% purity as assessed by analytical liquid chromatography using the following UPLC/MS method: column Acquity HSS T3 1.8 μm, 2.1 mm × 50 mm at 50 °C; eluent A, water + 0.05% formic acid + 3.75 mM ammonium acetate; eluent B, acetonitrile + 0.04% formic acid; gradient, from 2% to 98% B in 1.4 min; flow rate, 1.2 mL/min. High resolution mass analyses (HRMS) were performed by using electrospray ionization in positive mode after separation by liquid chromatography. The elemental composition was derived from the averaged mass spectra acquired at a high resolution of about 30 000 on an LTQ Orbitrap XL mass spectrometer (Thermo Scientific). The high mass accuracy below 1 ppm was obtained by using a lock mass.

***N*-Benzyl-3,5-dimethyl-*N*-phenylisoxazole-4-carboxamide (2).** *N*-Phenylbenzylamine (1.3 g, 7.02 mmol), EDC·HCl (1.66 g, 8.44 mmol), and triethylamine (1.18 mL, 8.42 mmol) were added to a solution of 3,5-dimethylisoxazole-4-carboxylic acid (1.0 g, 7.01 mmol) in dry dichloromethane (10 mL), and the resulting mixture was stirred for 22 h at rt. After that time, the reaction mixture was diluted with EtOAc (50 mL) and extracted with aqueous HCl solution (1 M, 20 mL), followed by a saturated aqueous $NaHCO_3$ solution (30 mL). The combined organic layers were dried ($MgSO_4$), and the solvent was removed under reduced pressure. The product was purified by flash chromatography using a heptane/EtOAc gradient to yield the title compound **2** (240 mg, 0.78 mmol, 11%). ^{1}H NMR (400 MHz, $CDCl_3$) δ 7.10−7.36 (m, 8H), 6.85−6.95 (m, 2H), 5.10 (s, 2H), 2.16 (s, 3H), 2.10 (s, 3H). UPLC/MS: 1.07 min, 307.2 $[M + H]^+$. HRMS (ESI^+) calcd for $C_{19}H_{19}N_2O_2$ $[M + H]^+$ 307.144 10, found 307.144 32.

***N*-Benzyl-*N*-phenylisonicotinamide (3).** Isonicotinic acid (500 mg, 4.06 mmol), PyBroP (4.10 g, 8.79 mmol), and triethylamine (1.13 ml, 8.08 mmol) were added to a solution of *N*-phenylbenzylamine (619 mg, 3.34 mmol) in dry dichloromethane (10 mL), and the resulting mixture was stirred for 22 h at rt. After that time, the reaction mixture was filtered through a syringe filter, and the filtrate was concentrated under reduced pressure. The residue was purified by preparative HPLC (Waters Sunfire C18 OBD 30 mm × 100 mm, flow 30 mL/min, water + 0.1% TFA and acetonitrile + 0.1% TFA gradient) to yield the title compound **3** (817 mg, 2.84 mmol, 85%). ^{1}H NMR (400 MHz, CD_3OD) δ 8.43−8.33 (m, 2H), 7.36−7.12 (m, 10H), 7.06−6.95 (m, 2H), 5.19−5.09 (s, 2H). UPLC/MS: 0.94 min, 289.2 $[M + H]^+$. HRMS (ESI^+) calcd for $C_{19}H_{17}N_2O$ $[M + H]^+$ 289.133 54, found 289.133 51.

***N*-Benzyl-2-methyl-*N*-phenylisonicotinamide (4).** 2-Methylisonicotinic acid (44 mg, 0.32 mmol) was dissolved in 500 μL of a freshly prepared 1-chloro-*N*,*N*,2-trimethylpropenylamine solution in dry dichloromethane (1 g/ml), and the resulting mixture was stirred for 2.5 h at rt. Next, a solution of *N*-phenylbenzylamine (30 mg, 0.162 mmol) and *N*,*N*-diisopropylethylamine (55 μL, 0.32 mmol) in 1 mL of dry dichloromethane was added, and the reaction mixture was then stirred for 1.5 h at rt. After that time, the reaction mixture was concentrated under reduced pressure. The residue was purified by preparative HPLC (Waters Sunfire C18 OBD 30 mm × 100 mm, flow 30 mL/min, water + 0.1% TFA and acetonitrile + 0.1% TFA gradient) to yield the title compound **4** (51 mg, 0.17 mmol, 53%). ^{1}H NMR (600 MHz, DMSO-d_6) δ 8.44 (s, 1H), 7.52 (br s, 1H), 7.13−7.33 (m, 11H), 5.11 (s, 2H), 2.47 (s, 3H). UPLC/MS: 0.93 min, 303.2 $[M + H]^+$. HRMS (ESI^+) calcd for $C_{20}H_{19}N_2O$ $[M + H]^+$ 303.149 19, found 303.149 21.

***N*-Benzyl-3-methyl-*N*-phenylisonicotinamide (5).** $POCl_3$ (2.37 mL, 25.7 mmol) and pyridine (9.4 mL, 117 mmol) were added to a stirred solution of *N*-phenylbenzylamine (4.27 g, 23.3 mmol) and 3-methylpyridine-4-carboxylic acid (3.20 g, 23.3 mmol) in dry dichloromethane (6 mL) at rt. The reaction mixture was heated at reflux temperature for 2 h. After that time, a saturated aqueous $NaHCO_3$ solution was added (50 mL), followed by the addition of dichloromethane (50 mL). The aqueous layer was extracted three times with dichloromethane. The combined organic layers were dried ($MgSO_4$), and the solvent was removed under reduced pressure. The product was purified by flash chromatography using a heptane/EtOAc gradient to yield the title compound **5** (6.14 g, 20.3 mmol, 87%). ^{1}H NMR (400 MHz, DMSO-d_6) δ 8.31 (s, 1H), 8.19 (d, J = 4.41 Hz, 1H), 7.22−7.38 (m, 5H), 6.99−7.20 (m, 6H), 5.11 (br s, 2H), 2.27 (s, 3H). UPLC/MS: 0.95 min, 303.2 $[M + H]^+$. HRMS (ESI^+) calcd for $C_{20}H_{19}N_2O$ $[M + H]^+$ 303.149 19, found 303.149 11.

***N*-Benzyl-4-methyl-*N*-phenylnicotinamide (6).** 1-Chloro-*N*,*N*,2-trimethylpropenylamine (116 μL, 0.87 mmol) was added to a solution of 4-methylnicotinic acid (80 mg, 0.583 mmol) in dry

dx.doi.org/10.1021/jm501052c | J. Med. Chem. XXXX, XXX, XXX−XXX

dichloromethane (5 mL), and the resulting pale yellow suspension was stirred for 10 min at rt. Next, a solution of *N*-phenylbenzylamine (128 mg, 0.7 mmol) and triethylamine (243 μL, 1.75 mmol) in dry THF (1 mL) was added, and the reaction mixture was stirred for 1 h at rt. After that time, the reaction mixture was diluted with 30 mL of dichloromethane, and the organic layer was extracted with a saturated aqueous $NaHCO_3$ solution (2 × 20 mL). The organic layer was dried (Na_2SO_4) and concentrated under reduced pressure. The residue was purified by preparative HPLC (Waters Sunfire C18 OBD 18 mm × 60 mm, flow 20 mL/min, water + 0.1% TFA and acetonitrile + 0.1% TFA gradient) to yield the title compound **6** (133 mg, 0.32 mmol, 55%). ^{1}H NMR (400 MHz, $CDCl_3$) δ 8.33−8.45 (m, 2H), 7.08−7.43 (m, 9H), 6.79−6.91 (m, 2H), 5.12 (s, 2H), 2.55 (s, 3H). UPLC/MS: 0.96 min, 303.2 $[M + H]^+$. HRMS (ESI^+) calcd for $C_{20}H_{19}N_2O$ $[M + H]^+$ 303.149 19, found 303.149 11.

Lithium 3-Methylpyridazine-4-carboxylate. A solution of 2-acetylpent-4-enoic acid ethyl ester (3.85 g, 22.6 mmol) and Sudan III (0.5 mg) in dry dichloromethane (30 mL) and methanol (3 mL) at −78 °C was subjected to a stream of O_3 in O_2 until the color change to blue was persistent. Next, an amount of 17.5 g of PL-TPP (polymer bound triphenylphosphine, loading 1.42 mmol/g, 24.8 mmol) was added, and the cooling bath was removed. After 1 h at rt, the reaction mixture was filtered and concentrated under reduced pressure, yielding 3-oxo-2-(2-oxoethyl)butyric acid ethyl ester (3.89 g, 22.6 mmol, 100%) which was used in the next step without further purification.

A solution of 3-oxo-2-(2-oxoethyl)butyric acid ethyl ester (3.64 g, 21.1 mmol) in ethanol (35 mL) was slowly treated with 724 μL of hydrazine hydrate in 10 mL of ethanol at 0 °C. The cooling bath was removed, and the reaction mixture was stirred for 2.5 h at rt. Next, a solution of sodium nitrite (2.21 g, 31.7 mmol) in 1 mL of H_2O followed by AcOH (7 mL) was added. After 1 h, a saturated aqueous solution of $NaHCO_3$ was added dropwise until gas formation stopped completely. The mixture was extracted with EtOAc (3 × 50 mL). The combined organic layers were dried (Na_2SO_4) and concentrated under reduced pressure. The product was purified by flash chromatography using a heptane/EtOAc gradient to give ethyl 3-methylpyridazine-4-carboxylate (1.0 g, 6.04 mmol, 28%). ^{1}H NMR (400 MHz, $CDCl_3$) δ 9.24 (d, *J* = 5.1 Hz, 1H), 7.83 (d, *J* = 5.1 Hz, 1H), 4.43 (q, *J* = 7.1 Hz, 2H), 2.99 (s, 3H), 1.42 (t, *J* = 7.1 Hz, 3H). ESI-MS 189 (M + Na).

A solution of of ethyl 3-methylpyridazine-4-carboxylate (704 mg, 4.23 mmol) in THF (2 mL) was treated with an aqueous solution of LiOH (2 M, 2.2 mL) and stirred for 1.5 h at rt. The reaction mixture was concentrated under reduced pressure yielding crude lithium 3-methylpyridazine-4-carboxylate which was used in the next step without further purification.

***N*-Benzyl-3-methyl-*N*-phenylpyridazine-4-carboxamide (7).** $POCl_3$ (42.3 μL, 0.45 mmol) and pyridine (126 μL, 117 mmol) were added to a stirred solution of *N*-phenylbenzylamine (4.27 g, 23.3 mmol) and lithium 3-methylpyridazine-4-carboxylate (50 mg, 0.352 mmol) in dry dichloromethane (5 mL) at rt. The reaction mixture was stirred for 2 h at rt. After that time, a saturated aqueous $NaHCO_3$ solution was added (20 mL), followed by the addition of dichloromethane (20 mL). The aqueous layer was extracted with dichloromethane (3 × 20 mL). The combined organic layers were dried ($MgSO_4$), and the solvent was removed under reduced pressure. The product was purified by flash chromatography using a heptane/EtOAc gradient to yield the title compound **7** (30 mg, 0.10 mmol, 28%). ^{1}H NMR (400 MHz, $CDCl_3$) δ 8.83 (d, *J* = 5.07 Hz, 1H), 7.22−7.35 (m, 8H), 7.10−7.17 (m, 1H), 6.98 (d, *J* = 5.07 Hz, 1H), 6.83 (dd, *J* = 3.20, 6.28 Hz, 1H), 5.11 (s, 2H), 2.75 (s, 3H). UPLC/MS: 0.89 min, 304.2 $[M + H]^+$. HRMS (ESI^+) calcd for $C_{19}H_{18}N_3O$ $[M + H]^+$ 304.144 44, found 304.144 56.

***N*-Benzyl-1,4-dimethyl-*N*-phenyl-1*H*-imidazole-5-carboxamide (8).** 1-Chloro-*N*,*N*,2-trimethylpropenylamine (138 μL, 1.02 mmol) was added to a solution of 3,5-dimethyl-3*H*-imidazole-4-carboxylic acid (101 mg, 0.72 mmol) in dry dichloromethane (4 ml), and the resulting suspension was stirred for 1 h at rt. Next, *N*-phenylbenzylamine (110 mg, 0.60 mmol) and triethylamine (252 μL, 1.80 mmol) were added, and the resulting reaction mixture was stirred for 2.5 h at rt. After that time, the reaction mixture was diluted with 5 mL of dichloromethane, and the organic layer was extracted with a saturated aqueous $NaHCO_3$ solution (2 × 5 mL). The organic layer was dried (Na_2SO_4) and concentrated under reduced pressure. The residue was purified by preparative HPLC (Waters Sunfire C18 OBD 18 mm × 60 mm, flow 20 mL/min, water + 0.1% TFA and acetonitrile + 0.1% TFA gradient) to yield the title compound **8** (73 mg, 0.24 mmol, 40%). ^{1}H NMR (400 MHz, DMSO-d_6) δ 7.51 (s, 1H), 7.02−7.35 (m, 10H), 5.13 (s, 2H), 3.67 (s, 3H), 1.64 (s, 3H). UPLC/MS: 0.72 min, 306.2 $[M + H]^+$. HRMS (ESI^+) calcd for $C_{19}H_{20}N_3O$ $[M + H]^+$ 306.160 09, found 306.160 19.

3-Methyl-*N*-phenethyl-*N*-phenylisonicotinamide (9). 3-Methylisonicotinic acid (137 mg, 1 mmol) was dissolved in of a freshly prepared solution of 1-chloro-*N*,*N*,2-trimethylpropenylamine in dry dichloromethane (1 g/mL, 1.5 mL), and the resulting mixture was stirred for 2.5 h at rt. Next, a solution of *N*-phenethylaniline (99 mg, 0.5 mmol) and *N*,*N*-diisopropylethylamine (171 μL, 1 mmol) in dry dichloromethane (1 mL) was added and stirring was continued for 2 h at rt. After that time, the reaction mixture was concentrated under reduced pressure. The residue was purified by preparative HPLC (Waters Sunfire C18 OBD 30 mm × 100 mm, flow 30 mL/min, water + 0.1% TFA and acetonitrile + 0.1% TFA gradient) to yield the title compound **9** (39 mg, 0.12 mmol, 12%). ^{1}H NMR (600 MHz, DMSO-d_6) δ 8.44 (s, 1H), 8.32 (br s, 1H), 7.13−7.32 (m, 11H), 4.16 (t, *J* = 7.3 Hz, 2H), 2.91 (t, *J* = 7.3 Hz, 2H), 2.21 (s, 3H). UPLC/MS: 1.01 min, 317.2 $[M + H]^+$. HRMS (ESI^+) calcd for $C_{21}H_{21}N_2O$ $[M + H]^+$ 317.164 84, found 317.164 82.

***N*,*N*-Dibenzyl-3-methylisonicotinamide (10).** $POCl_3$ (75.0 μL, 0.82 mmol) and pyridine (202 μL, 2.50 mmol) were added to a stirred solution of dibenzylamine (96 μL, 0.50 mmol) and 3-methylpyridine-4-carboxylic acid (68.5 mg, 0.50 mmol) in dry dichloroethane (2 mL) at rt. The reaction mixture was heated to reflux in a microwave reactor for 10 min. After that time, a saturated aqueous $NaHCO_3$ solution was added (10 mL), followed by the addition of dichloromethane (10 mL). The aqueous layer was extracted with dichloromethane (3 × 10 mL). The combined organic layers were dried ($MgSO_4$), and the solvent was removed under reduced pressure. The residue was purified by preparative HPLC (Waters Sunfire C18 OBD 18 mm × 60 mm, flow 20 mL/min, water + 0.1% TFA and acetonitrile + 0.1% TFA gradient) to yield the title compound **10** (114 mg, 0.36 mmol, 72%). ^{1}H NMR (400 MHz, DMSO-d_6) δ 8.48 (s, 1H), 8.42 (d, *J* = 4.89 Hz, 1H), 7.26−7.42 (m, 8H), 7.23 (d, *J* = 4.89 Hz, 1H), 7.09 (br s, 2H), 4.69 (br s, 2H), 4.29 (br s, 2H), 2.19 (s, 3H). UPLC/MS: 1.01 min, 317.2 $[M + H]^+$. HRMS (ESI^+) calcd for $C_{21}H_{21}N_2O$ $[M + H]^+$ 317.164 84, found 317.164 89.

***N*-Isobutyl-3-methyl-*N*-phenylisonicotinamide (11).** $POCl_3$ (68.2 μL, 0.74 mmol) and pyridine (269 μL, 3.35 mmol) were added to a stirred solution of *N*-(2-methylpropyl)aniline (100 mg, 0.67 mmol) and 3-methylpyridine-4-carboxylic acid (92 mg, 0.67 mmol) in dry dichloromethane (2 mL) at rt. The reaction mixture was heated at reflux temperature for 1.5 h. After that time, a saturated aqueous $NaHCO_3$ solution was added (10 mL), followed by the addition of dichloromethane (10 mL). The aqueous layer was extracted with dichloromethane (3 × 10 mL). The combined organic layers were dried ($MgSO_4$), and the solvent was removed under reduced pressure. The residue was purified by preparative HPLC (Waters Sunfire C18 OBD 18 mm × 60 mm, flow 20 mL/min, water + 0.1% TFA and acetonitrile + 0.1% TFA gradient) to yield the title compound **11** (31 mg, 0.12 mmol, 17%). ^{1}H NMR (400 MHz, DMSO-d_6) δ 8.29 (s, 1H), 8.15 (d, *J* = 4.63 Hz, 1H), 7.12−7.28 (m, 5H), 7.01 (d, *J* = 4.85 Hz, 1H), 3.75 (d, *J* = 7.28 Hz, 2H), 2.24 (s, 3H), 1.65−1.78 (m, 1H), 0.93 (d, *J* = 6.62 Hz, 6H). UPLC/MS: 0.93 min, 269.2 $[M + H]^+$. HRMS (ESI^+) calcd for $C_{17}H_{21}N_2O$ $[M + H]^+$ 269.164 84, found 269.164 89.

***N*-(2-Methoxybenzyl)-3-methyl-*N*-phenylisonicotinamide (12).** 3-Methylisonicotinic acid (137 mg, 1 mmol) was dissolved in a freshly prepared 1-chloro-*N*,*N*,2-trimethylpropenylamine solution in dry dichloromethane (1 g/mL, 1.5 mL), and the resulting mixture was stirred for 2.5 h at rt. Next, a solution of *N*-phenethylaniline (99 mg, 0.5 mmol) and *N*,*N*-diisopropylethylamine (171 μL, 1 mmol) in dry dichloromethane (1 mL) was added. The resulting solution was then

stirred for 2 h at rt. After that time, the reaction mixture was concentrated under reduced pressure. The residue was purified by preparative HPLC (Waters Sunfire C18 OBD 30 mm × 100 mm, flow 30 mL/min, water + 0.1% TFA and acetonitrile + 0.1% TFA gradient) to yield the title compound **12** (40 mg, 0.12 mmol, 12%). ^{1}H NMR (600 MHz, DMSO-d_6) δ 8.44 (1H), 7.52 (br s, 1H), 7.13−7.33 (10 H), 5.13 (s, 2H), 3.70 (s, 3H), 2.37 (s, 3H). UPLC/MS: 0.94 min, 333.2 $[M + H]^+$. HRMS (ESI^+) calcd for $C_{21}H_{21}N_2O_2$ $[M + H]^+$ 333.159 75, found 333.159 75.

***N*-(2-Methoxybenzyl)-2-(trifluoromethoxy)aniline.** 2-(Trifluoromethoxy)aniline (156 g, 0.88 mmol) and sodium triacetoxyborohydride (328 mg, 1.47 mmol) were added to a solution of 2-methoxybenzaldehyde (100 mg, 0.73 mmol) in dry dichloromethane (1 mL), and the resulting mixture was stirred 2 h at rt. After that time, a saturated aqueous $NaHCO_3$ solution was added dropwise until gas evolution had stopped. The mixture was diluted with EtOAc (5 mL) and washed with saturated aqueous $NaHCO_3$ solution. The organic layer was dried (Na_2SO_4) and concentrated under reduced pressure. The product was purified by flash chromatography using a heptane/EtOAc gradient to give *N*-(2-methoxybenzyl)-2-(trifluoromethoxy)-aniline (163 mg, 0.55 mmol, 75%). ^{1}H NMR (400 MHz, DMSO-d_6) δ 7.26−7.18 (m, 1H), 7.15 (dd, J = 7.9, 1.7 Hz, 2H), 7.09−7.02 (m, 1H), 7.00 (d, J = 8.2 Hz, 1H), 6.88−6.82 (m, 1H), 6.56 (td, J = 7.7, 1.4 Hz, 1H), 6.51 (dd, J = 8.2, 1.4 Hz, 1H), 6.15 (t, J = 6.2 Hz, 1H), 4.32 (d, J = 6.2 Hz, 2H), 3.85 (s, 3H).

***N*-(2-Methoxybenzyl)-3-methyl-*N*-(2-(trifluoromethoxy)-phenyl)isonicotinamide (13).** 1-Chloro-*N*,*N*,2-trimethylpropenylamine (68 μL, 0.51 mmol) was added to a solution of 3-methylisonicotinic acid (90 mg, 0.30 mmol) in dry dichloromethane (3 mL), and the resulting mixture was stirred for 1 h at rt. Next, *N*-(2-methoxybenzyl)-2-(trifluoromethoxy)aniline (49.8 mg, 0.36 mmol) and *N*,*N*-diisopropylethylamine (127 μL, 0.91 mmol) were added, and the resulting solution was then stirred for 2 h at rt. After that time, the reaction mixture was diluted with dichloromethane (5 mL) and washed with a saturated aqueous $NaHCO_3$ solution. The organic layer was dried (Na_2SO_4) and concentrated under reduced pressure. The residue was purified by preparative HPLC (Waters Sunfire C18 OBD 18 mm × 60 mm, flow 20 mL/min, water + 0.1% TFA and acetonitrile + 0.1% TFA gradient) to give the title compound **13** (76 mg, 0.18 mmol, 60%). ^{1}H NMR (400 MHz, DMSO-d_6, 4:1 mixture of rotamers, data given for major isomer) δ 8.37 (s, 1H), 8.16 (d, J = 4.85 Hz, 1H), 7.09−7.31 (m, 6H), 6.84−6.98 (m, 3H), 5.27 (d, J = 14.33 Hz, 1H), 4.76 (d, J = 14.33 Hz, 1H), 3.62 (s, 3H), 2.30 (s, 3H). UPLC/MS: 1.12 min, 417.2 $[M + H]^+$. HRMS (ESI^+) calcd for $C_{22}H_{20}F_3N_2O_3$ $[M + H]^+$ 417.142 05, found 417.141 88.

***N*-(3,5-Dichlorophenyl)-*N*-(2-methoxybenzyl)-3-methylisonicotinamide (14).** 1-Chloro-*N*,*N*,2-trimethylpropenylamine (320 μL, 2.42 mmol) was added to a solution of 3-methylisonicotinic acid (150 mg, 1.09 mmol) in dry dichloromethane (10 mL), and the resulting mixture was stirred for 45 min at rt. Next, 3,5-dichloro-*N*-(2-methoxybenzyl)aniline (339 mg, 1.2 mmol) and *N*,*N*-diisopropylethylamine (457 μL, 3.27 mmol) were added, and the resulting solution was then stirred for 30 min at rt. After that time, the reaction mixture was diluted with dichloromethane (5 mL) and washed with a saturated aqueous $NaHCO_3$ solution. The organic layer was dried (Na_2SO_4) and concentrated under reduced pressure. The product was purified by flash chromatography using a heptane/EtOAc gradient to yield the title compound **14** (380 mg, 0.95 mmol, 87%). ^{1}H NMR (400 MHz, CD_3OD) δ 8.37 (br s, 1H), 8.21−8.29 (m, 1H), 6.81−7.42 (m, 8H), 5.19 (br s, 2H), 3.74 (s, 3H), 2.37 (s, 3H). UPLC/MS: 1.16 min, 401.1 $[M + H]^+$. HRMS (ESI^+) calcd for $C_{21}H_{19}Cl_2N_2O_2$ $[M + H]^+$ 401.081 81, found 401.081 70.

4-Fluoro-2-methyl-*N*-((2-methyl-1*H*-indol-4-yl)methyl)-aniline. Dibutyltin dichloride (191 mg, 0.63 mmol) was added to a solution of 2-methyl-1*H*-indole-4-carbaldehyde (1.00 g, 6.28 mmol) and 4-fluoro-2-methylaniline (1.18 g, 9.42 mmol) in THF (15 mL), and the resulting reaction mixture was stirred for 15 min at rt. Next, phenylsilane (2.72 g, 25.1 mmol) was added, and stirring was continued for 1 h at rt. After that time, the reaction mixture was diluted with EtOAc (80 mL) and washed with a saturated aqueous $NaHCO_3$ solution (2 × 30 mL). The organic layer was dried (Na_2SO_4) and concentrated under reduced pressure. The product was purified by flash chromatography using a cyclohexane/EtOAc gradient to give 4-fluoro-2-methyl-*N*-((2-methyl-1*H*-indol-4-yl)methyl)aniline (1.23 g, 3.90 mmol, 62%). ^{1}H NMR (400 MHz, $CDCl_3$) δ 7.95 (br s, 1H), 7.29−7.20 (m, 1H), 7.14−7.04 (m, 2H), 6.81 (ddd, J = 8.8, 6.1, 3.1 Hz, 2H), 6.62 (dd, J = 9.7, 4.8 Hz, 1H), 6.34−6.29 (m, 1H), 4.54 (s, 2H), 3.73 (br s, 1H), 2.47 (d, J = 1.0 Hz, 3H), 2.12 (s, 3H).

***N*-(4-Fluoro-2-methylphenyl)-3-methyl-*N*-((2-methyl-1*H*-indol-4-yl)methyl)isonicotinamide (15).** 3-Methylisonicotinic acid (350 mg, 2.55 mmol) and pyridine (1.03 mL, 12.76 mmol) were added to a solution of 4-fluoro-2-methyl-*N*-((2-methyl-1*H*-indol-4-yl)methyl)aniline (1.21 g, 3.83 mmol) in dry THF (40 mL). At 0 °C, a solution of $POCl_3$ (509 mg, 3.32 mmol) in THF (1 mL) was added dropwise. The cooling bath was removed, and the reaction mixture was stirred for 1.5 h at rt. After that time, the reaction mixture was diluted with EtOAc (50 mL), washed with a saturated aqueous $NaHCO_3$ solution (50 mL). The organic layer was dried (Na_2SO_4) and concentrated under reduced pressure. The residue was purified by preparative HPLC (Waters Sunfire C18 OBD 18 mm × 150 mm, flow 20 mL/min, water + 0.1% TFA and acetonitrile + 0.1% TFA gradient) to yield the title compound **15** (370 mg, 0.91 mmol, 35%). ^{1}H NMR (400 MHz, $CDCl_3$) δ 8.32 (s, 1H), 8.14 (d, J = 5.07 Hz, 1H), 7.95 (br s, 1H), 7.22 (d, J = 8.16 Hz, 1H), 6.89−6.95 (m, 1H), 6.79 (d, J = 5.07 Hz, 1H), 6.64−6.73 (m, 2H), 6.38−6.46 (m, 3H), 5.81 (d, J = 13.67 Hz, 1H), 4.73 (d, J = 13.67 Hz, 1H), 2.46 (s, 3H), 2.36 (s, 3H), 2.08 (s, 3H). UPLC/MS: 1.00 min, 388.2 $[M + H]^+$. HRMS (ESI^+) calcd for $C_{24}H_{23}FN_3O$ $[M + H]^+$ 388.18197, found 388.18188.

Biology. All aspects of animal care, use, and welfare for research animals used for in vivo studies were performed in compliance with local governmental regulations. Furthermore, all animals were handled in accordance with Novartis Animal Care and Use Committee approved protocols and regulations.

Cell Culture. Stable Jurkat cell lines expressing GPBAR1 were cultured as suspensions in T175 cc flasks at 37 °C, 5% CO_2, and 95% relative humidity in AIM-V serum-free medium (GIBCO BRL) supplemented with 1% penicillin (stock solution 100IE/ml) and 1% streptomycin (stock solution 100 μg/mL, Gibco BRL), 2 mM glutamine, and 1 μg/mL puromycin (Sigma). Cells were passaged every second day, and cell density was always kept below 1 × 10^6 cells per mL of medium, in particular at harvesting before running the calcium assay. Cells were split every 2−3 days with a ratio of 1:3 to 1:4.

GPBAR1 Cellular cAMP Assay. Jurkat cells overexpressing human or mouse GPBAR1 were seeded at (50 000 cells/25 μL)/well in 384-well plates (Greiner) in AIM V medium (Life Technologies) supplemented with 1 mM IBMX (Sigma) and 10 mM HEPES. Immediately after plating, an amount of 200 nL of compounds in DMSO was transferred using the Pintool (GNF systems). After 1 h at 37 °C, cryptate and D2 conjugates from the cAMP HiRange HTRF kit (Cisbio) were added (12.5 μL each). Plates were then incubated 1 h at rt, and emission at 620 and 665 nm was read on the Envision (PerkinElmer) as suggested by the manufacturer. Data were expressed as a ratio of emission at 665/620 and then normalized to a DMSO alone control. Dose−response data points were curve fitted using the standard logistic regression model. The percent efficacy was then determined based on *N*-(3,5-dichlorophenyl)-*N*-(1-(2-methoxyphenyl)ethyl)-3-methylisonicotinamide[35] as the internal control. The resultant EC_{50} values correspond to the compound concentration that displaces 50% of the binding of the d2-labeled cAMP.

GPBAR1 Calcium Mobilization Assay. Experiments were run using two different plate formats. The miniaturized 384-well format was used in HTS, whereas the 96-well format was used from hit-to-lead stage onward.

For the 96-well protocol, Jurkat cells expressing either human or mouse GPBAR1 were harvested from tissue culture flasks by centrifugation at 200*g* and resuspended in Fluo-4 AM dye loading solution (3 mL per 1 × 10^7 cells containing 1 μM Fluo-4 AM, 2 mM probenicid in complete RPMI medium buffered with 20 mM HEPES,

pH 7.4) on the day of the experiment. After incubation for 1 h at 37 °C, cells were washed twice with 10 mL of assay buffer containing 2 mM probenecid (centrifugation at 200*g*). Cells were then counted and transferred into black/clear bottom 96-well plates at 2×10^5 cells per well in 75 μL of assay buffer. Assay plates were centrifuged for 2 min at 200*g* before use on the FLIPR instrument (FLIPR I instrument, Molecular Devices, Sunnyvale, CA, USA).

For the 384-well protocol, Jurkat cells expressing human GPBAR1 were harvested from cell culture flasks, counted, and adjusted to 2×10^6 cells per mL of assay buffer. An aliquot of 20 μL per well was then dispensed in 384-well assay plates (black with clear bottom, Corning, USA) and plates were centrifuged for 3 min at 1200 rpm. After incubation at 37 °C in a humidified atmosphere for 30 min, cells were stained by dispensing 20 μL of loading solution containing Fluo-4 2-fold concentrated into wells, and incubating plates for 1 h at 37 °C. Subsequently, cells were washed using an EMBLA cell plate washer. After the last wash, a volume of 20 μL of assay buffer was left over the cell monolayer. Cells were then allowed to stabilize for 15−20 min before starting measurements on the FLIPR II instrument (Molecular Devices). Data were expressed as a normalized fluorescence ratio ($\Delta F/F = (F_{max} - F_b)/F_b$) where F_b corresponds to *f* values prior to agonist (TLCA) or compound injection and F_{max} to the fluorescence at the signal peak. Data were then normalized to TLCA values.

Human Monocyte Isolation, Differentiation, and Activation. Human peripheral blood mononuclear cells (PBMCs) were isolated from blood of healthy volunteers (Blutspendezentrum Basel) by density gradient centrifugation over Ficoll-Paque PLUS (GE Healthcare) using 50 mL Leucosep tubes (Greiner Bio-One). Subsequently, monocytes were isolated from PBMCs by magnetic removal of complementary leukocyte lineages using an untouched monocyte kit on a RoboSep instrument (both from Stemcell Technologies). Purified monocytes were differentiated into macrophages by 6 days culture in complete medium (CM) consisting of RPMI 1640 Glutamax medium supplemented with 10% fetal calf serum (PAA Laboratories), 10 μg/mL penicillin/streptomycin, 1 mM sodium pyruvate, 25 mM HEPES, and 50 μM β-mercaptoethanol, all from Life Technologies. Isolated monocytes were stimulated overnight with 10 ng/mL LPS (Sigma) in the presence of the indicated compounds or control (DMSO), and cytokine production was assessed by specific ELISA Ready-SET-Go kits (Affymetrix-eBioscience).

For M0/M1/M2 phenotyping experiments, isolated monocytes were differentiated into macrophages subsets by culturing them for 6 additional days at 2.5×10^6 cells/well in 6-well tissue culture plates (Corning Costar) in the presence of 40 ng/mL M-CSF for M0 differentiation, 40 ng/mL M-CSF with 50 ng/mL IFN-γ for M1 differentiation, or 40 ng/mL M-CSF with 50 ng/mL IL-4 for M2 differentiation, cytokine cocktails (all from R & D Systems) in the presence of indole **15** (3 uM) or control DMSO. At day 6, an aliquot of 1×10^6 cells from each condition was used to evaluate surface markers by mass cytometry using a CyTOF instrument (DVS-Fluidigm).

At day 7, the remaining differentiated macrophages were stimulated during 2 h with 10 ng/mL LPS (Sigma) in the presence of test compound or control (DMSO) and subsequently supplemented overnight with brefeldin A (Affymetrix eBioscience) to avoid secretion of produced cytokines. At day 8, the cells were analyzed for extracellular and intracellular markers by mass cytometry using a CyTOF instrument.

Staining of Cell for Mass Cytometry. Metal-labeled antibodies were prepared using MAXPAR antibody labeling kit (DVS Sciences) according to the manufacturer's protocol. The following antibody/labels (100 μL/2.5×10^6 cells) were used: anti-CD25 (eBioscience)/La^{139}, anti-TNF-α (R&D)/Nd^{143}, anti-IL-23p19 (R&D)/Sm^{147}, anti-CD40 (Biolegend)/Nd^{148}, anti-IL-6 (Biolegend)/Sm^{149}, anti-CD200R (Biolegend)/Sm^{152}, anti-IL-10 (R&D)/Eu^{153}, anti-CD45 (DVS)/Sm^{154}, anti-CD33 (DVS)/Gd^{158} or anti-IFN-γ (Biolegend)/Gd^{158}, anti-CD11c (DVS)/Tb^{159}, anti-CD14 (Biolegend)/Gd^{160}, anti-IL-1β (R&D)/Dy^{162}, anti-CD38 (Biolegend)/Er^{167}, anti-CD206 (Biolegend)/Er^{168}, anti-CD71 (Biolegend)/Tm^{169}, anti-CCL18 (Leinco)/Er^{170}, anti-CD64 (Biolegend)/Yb^{171}, anti-IL-12p40 (R&D)/Yb^{172}, anti-HLA-DR (DVS)/Yb^{174}, and anti-CD303 (Miltenyi)/Lu^{175}. Cisplatin solution (Enzo Life Sciences) was used at 25 mM final concentration. DNA intercalator $Ir^{191/193}$ (DVS Sciences) was used at 1:2000. CyTOF buffer consisted of PBS/CMF + 0.1% BSA + 2 mM EDTA + 0.01% NaN_3. Tru-Stain fcx (anti-human CD16/32, BioLegend) was used at 5 μL per 1×10^6 cells in CyTOF buffer to block unspecific binding of the antibodies. Permeabilization buffer for cytokine staining was purchased from eBioscience.

Cell cultures were harvested into a 15 mL tube and spun down to discard supernatants. Subsequently, they were washed twice with 1 mL of CyTOF buffer and transferred separately into 1.5 mL Eppendorf tubes, where they were resuspended and incubated with cisplatin solution for 1 min. Cells were spun down again and exposed to 500 μL of Fc block solution for 5 min at 4 °C. Subsequently, cells were stained with antibody cocktails in 100 μL of CyTOF buffer by incubating them during 30 min at 4 °C after gently vortexing the samples. After two additional washes, the cells were fixed adding 100 μL per condition fixation solution (Phosphotop, Roche) during 15 min at rt. After two more washes, the cells were stained with intracellular staining cocktail during 1 h at 4 °C. Following the incubation, the cells were resuspended again, and 500 μL of intercalation solution was added and incubated during 15 min at rt. Cells were washed once more and incubated 15 min at rt with 70% methanol to achieve dehydratation. After a final wash with CyTOF buffer, the cells were spun down and the pelleted cells were adjusted at 1×10^6 per mL concentration with CyTOF buffer immediately prior to CyTOF acquisition.

Cells were analyzed on a CyTOF mass cytometer (DVS Sciences) at an event rate of around 500 cells per second. The initial settings and parameters of the instrument were set according to DVS process and recommendations. Before gating of the cell subpopulations, generated FCS files were normalized using a standard protocol provided by the Nolan lab (Stanford University).[36] Analysis, including cell density plots, heat maps, and SPADE were created in Cytobank (http://www.cytobank.org/).

LPS Induced Cytokine Release in Mice. WT animals were obtained from Jackson laboratories (C57BL/6). GPBAR1 knockout mice were obtained from Taconic (catalog no. TF0504, USA) and back-crossed to get B6 background before use in experiments. Male WT and KO mice (7−12 weeks old, 8−9 mice/group) were treated with vehicle, dexamethasone (5 mg/kg), or indole **15** (50 mg/kg, 10 mL/kg, po) 2 h before the LPS challenge. Vehicle formulation used was 45% Cremophor RH40, 36% corn oil glycerides, 9% propylene glycerol, and 10% ethanol. Following drug treatment, all animals were challenged with 40 μg/kg of LPS in saline ip. Whole blood was collected 90 min after injection. All collected blood was stored at room temperature until separation. Once centrifuged, the resulting serum was drawn off into a labeled 96-well plate and stored at −80 °C until analyzed. Sera were analyzed for TNF-α, IL12-p70, IL-10, IL-1β, IL-6, mKC, and IFN-γ using MSD multiplex Elisa kit.

■ ASSOCIATED CONTENT

Ⓢ Supporting Information

Surface analysis results, intensity heat maps, and a complete list of safety panel assays. This material is available free of charge via the Internet at http://pubs.acs.org.

■ AUTHOR INFORMATION

Corresponding Author

*E-mail: klemens.hoegenauer@novartis.com. Phone: 0041613246225.

Present Address

⊥D.G.N.: Organovo Holdings Inc., 6275 Nancy Ridge Drive, Suite 110, San Diego, CA 92121.

Notes

The authors declare no competing financial interest.

■ ACKNOWLEDGMENTS

We thank R. Kühr, P. Schmid, M. Boras, F. Amberger, R. Scheinecker, P. Nganga, Y. Regereau, and K.-S. Tücking (synthetic support); R. Feifel, S. Desrayaud, P. Guntz, L. Hoffmann, G. Laue, Y. Chen, G. Welzel, H. Sullivan, L. Tenaillon, A. Marcel, and J. Lehmann (in vitro and in vivo studies); R. Embacher, S. Guldbrandsen, and C. Schwärzler (CyTOF assistance and sample acquisition).

■ ABBREVIATIONS USED

BA, bile acid; DC, dendritic cell; dn, dose normalized; FLIPR, fluorometric imaging plate reader; GLP-1, glucagon-like peptide 1; GPBAR1, G-protein-coupled bile acid receptor 1; HT-logP, high-throughput log *P*; KO, knockout; LipE, lipophilicity efficiency; LPS, lipopolysaccharide; PBMC, peripheral blood mononuclear cell; rt, room temperature; TGR5, Takeda G-protein-coupled receptor 5; TLCA, taurolitocholic acid; TLC, thin layer chromatography; WT, wild type

■ REFERENCES

(1) Kawamata, Y.; Fujii, R.; Hosoya, M.; Harada, M.; Yoshida, H.; Miwa, M.; Fukusumi, S.; Habata, Y.; Itoh, T.; Shintani, Y.; Hinuma, S.; Fujisawa, Y.; Fujino, M. A G Protein-Coupled Receptor Responsive to Bile Acids. *J. Biol. Chem.* **2003**, *278*, 9435−9440.

(2) Schaap, F. G.; Trauner, M.; Jansen, P. L. M. Bile Acid Receptors as Targets for Drug Development. *Nat. Rev. Gastroenterol. Hepatol.* **2014**, *11*, 55−67.

(3) Pols, T. W. H.; Noriega, L. G.; Nomura, M.; Auwerx, J.; Schoonjans, K. The Bile Acid Membrane Receptor TGR5 as an Emerging Target in Metabolism and Inflammation. *J. Hepatol.* **2011**, *54*, 1263−1272.

(4) Evans, K. A.; Budzik, B. W.; Ross, S. A.; Wisnoski, D. D.; Jin, J.; Rivero, R. A.; Vimal, M.; Szewczyk, G. R.; Jayawickreme, C.; Moncol, D. L.; Rimele, T. J.; Armour, S. L.; Weaver, S. P.; Griffin, R. J.; Tadepalli, S. M.; Jeune, M. R.; Shearer, T. W.; Chen, Z. B.; Chen, L.; Anderson, D. L.; Becherer, J. D.; De Los Frailes, M.; Colilla, F. J. Discovery of 3-Aryl-4-isoxazolecarboxamides as TGR5 Receptor Agonists. *J. Med. Chem.* **2009**, *52*, 7962−7965.

(5) Pellicciari, R.; Gioiello, A.; Macchiarulo, A.; Thomas, C.; Rosatelli, E.; Natalini, B.; Sardella, R.; Pruzanski, M.; Roda, A.; Pastorini, E.; Schoonjans, K.; Auwerx, J. Discovery of 6α-Ethyl-23(*S*)-methylcholic Acid (S-EMCA, INT-777) as a Potent and Selective Agonist for the TGR5 Receptor, a Novel Target for Diabesity. *J. Med. Chem.* **2009**, *52*, 7958−7961.

(6) Budzik, B. W.; Evans, K. A.; Wisnoski, D. D.; Jin, J.; Rivero, R. A.; Szewczyk, G. R.; Jayawickreme, C.; Moncol, D. L.; Yu, H. Synthesis and Structure−Activity Relationships of a Series of 3-Aryl-4-isoxazolecarboxamides as a New Class of TGR5 Agonists. *Bioorg. Med. Chem. Lett.* **2010**, *20*, 1363−1367.

(7) Herbert, M. R.; Siegel, D. L.; Staszewski, L.; Cayanan, C.; Banerjee, U.; Dhamija, S.; Anderson, J.; Fan, A.; Wang, L.; Rix, P.; Shiau, A. K.; Rao, T. S.; Noble, S. A.; Heyman, R. A.; Bischoff, E.; Guha, M.; Kabakibi, A.; Pinkerton, A. B. Synthesis and SAR of 2-Aryl-3-aminomethylquinolines as Agonists of the Bile Acid Receptor TGR5. *Bioorg. Med. Chem. Lett.* **2010**, *20*, 5718−5721.

(8) Gioiello, A.; Rosatelli, E.; Nuti, R.; Macchiarulo, A.; Pellicciari, R. Patented TGR5 Modulators: A Review (2006 − Present). *Expert Opin. Ther. Pat.* **2012**, *22*, 1399−1414.

(9) Duan, H.; Ning, M.; Chen, X.; Zou, Q.; Zhang, L.; Feng, Y.; Zhang, L.; Leng, Y.; Shen, J. Design, Synthesis, and Antidiabetic Activity of 4-Phenoxynicotinamide and 4-Phenoxypyrimidine-5-carboxamide Derivatives as Potent and Orally Efficacious TGR5 Agonists. *J. Med. Chem.* **2012**, *55*, 10475−10489.

(10) Futatsugi, K.; Bahnck, K. B.; Brenner, M. B.; Buxton, J.; Chin, J. E.; Coffey, S. B.; Dubins, J.; Flynn, D.; Gautreau, D.; Guzman-Perez, A.; Hadcock, J. R.; Hepworth, D.; Herr, M.; Hinchey, T.; Janssen, A. M.; Jennings, S. M.; Jiao, W.; Lavergne, S. Y.; Li, B.; Li, M.; Munchhof, M. J.; Orr, S. T. M.; Piotrowski, D. W.; Roush, N. S.; Sammons, M.; Stevens, B. D.; Storer, G.; Wang, J.; Warmus, J. S.; Wei, L.; Wolford, A. C. Optimization of Triazole-Based TGR5 Agonists towards Orally Available Agents. *MedChemComm* **2012**, *4*, 205−210.

(11) Piotrowski, D. W.; Futatsugi, K.; Warmus, J. S.; Orr, S. T. M.; Freeman-Cook, K. D.; Londregan, A. T.; Wei, L.; Jennings, S. M.; Herr, M.; Coffey, S. B.; Jiao, W.; Storer, G.; Hepworth, D.; Wang, J.; Lavergne, S. Y.; Chin, J. E.; Hadcock, J. R.; Brenner, M. B.; Wolford, A. C.; Janssen, A. M.; Roush, N. S.; Buxton, J.; Hinchey, T.; Kalgutkar, A. S.; Sharma, R.; Flynn, D. A. Identification of Tetrahydropyrido[4,3-*d*]pyrimidine Amides as a New Class of Orally Bioavailable TGR5 Agonists. *ACS Med. Chem. Lett.* **2013**, *4*, 63−68.

(12) Londregan, A. T.; Piotrowski, D. W.; Futatsugi, K.; Warmus, J. S.; Boehm, M.; Carpino, P. A.; Chin, J. E.; Janssen, A. M.; Roush, N. S.; Buxton, J.; Hinchey, T. Discovery of 5-Phenoxy-1,3-dimethyl-1*H*-pyrazole-4-carboxamides as Potent Agonists of TGR5 via Sequential Combinatorial Libraries. *Bioorg. Med. Chem. Lett.* **2013**, *23*, 1407−1411.

(13) Martin, R. E.; Bissantz, C.; Gavelle, O.; Kuratli, C.; Dehmlow, H.; Richter, H. G. F.; Obst Sander, U.; Erickson, S. D.; Kim, K.; Pietranico-Cole, S. L.; Alvarez-Sánchez, R.; Ullmer, C. 2-Phenoxy-nicotinamides Are Potent Agonists at the Bile Acid Receptor GPBAR1 (TGR5). *ChemMedChem* **2013**, *8*, 569−576.

(14) Dehmlow, H.; Alvarez Sánchez, R.; Bachmann, S.; Bissantz, C.; Bliss, F.; Conde-Knape, K.; Graf, M.; Martin, R. E.; Obst Sander, U.; Raab, S.; Richter, H. G. F.; Sewing, S.; Sprecher, U.; Ullmer, C.; Mattei, P. Discovery and Optimisation of 1-Hydroxyimino-3,3-diphenylpropanes, a New Class of Orally Active GPBAR1 (TGR5) Agonists. *Bioorg. Med. Chem. Lett.* **2013**, *23*, 4627−4632.

(15) Zhu, J.; Ning, M.; Guo, C.; Zhang, L.; Pan, G.; Leng, Y.; Shen, J. Design, Synthesis and Biological Evaluation of a Novel Class of Potent TGR5 Agonists Based on a 4-Phenyl Pyridine Scaffold. *Eur. J. Med. Chem.* **2013**, *69*, 55−68.

(16) Zou, Q.; Duan, H.; Ning, M.; Liu, J.; Feng, Y.; Zhang, L.; Zhu, J.; Leng, Y.; Shen, J. 4-Benzofuranyloxynicotinamide Derivatives Are Novel Potent and Orally Available TGR5 Agonists. *Eur. J. Med. Chem.* **2014**, *82*, 1−15.

(17) Phillips, D. P.; Gao, W.; Yang, Y.; Zhang, G.; Lerario, I. K.; Lau, T. L.; Jiang, J.; Wang, X.; Nguyen, D. G.; Bhat, B. G.; Trotter, C.; Sullivan, H.; Welzel, G.; Landry, J.; Chen, Y.; Joseph, S. B.; Li, C.; Gordon, W. P.; Richmond, W.; Johnson, K.; Bretz, A.; Bursulaya, B.; Pan, S.; McNamara, P.; Seidel, H. M. Discovery of Trifluoromethyl-(pyrimidin-2-yl)azetidine-2-carboxamides as Potent, Orally Bioavailable TGR5 (GPBAR1) Agonists: Structure−Activity Relationships, Lead Optimization, and Chronic in Vivo Efficacy. *J. Med. Chem.* **2014**, *57*, 3263−3282.

(18) Keitel, V.; Donner, M.; Winandy, S.; Kubitz, R.; Häussinger, D. Expression and Function of the Bile Acid Receptor TGR5 in Kupffer Cells. *Biochem. Biophys. Res. Commun.* **2008**, *372*, 78−84.

(19) Pols, T. W. H.; Nomura, M.; Harach, T.; Lo Sasso, G.; Oosterveer, M. H.; Thomas, C.; Rizzo, G.; Gioiello, A.; Adorini, L.; Pellicciari, R.; Auwerx, J.; Schoonjans, K. TGR5 Activation Inhibits Atherosclerosis by Reducing Macrophage Inflammation and Lipid Loading. *Cell Metab.* **2011**, *14*, 747−757.

(20) Pols, T. W. H. TGR5 in Inflammation and Cardiovascular Disease. *Biochem. Soc. Trans.* **2014**, *42*, 244−249.

(21) Ichikawa, R.; Takayama, T.; Yoneno, K.; Kamada, N.; Kitazume, M. T.; Higuchi, H.; Matsuoka, K.; Watanabe, M.; Itoh, H.; Kanai, T.; Hisamatsu, T.; Hibi, T. Bile Acids Induce Monocyte Differentiation toward Interleukin-12 Hypo-Producing Dendritic Cells via a TGR5-Dependent Pathway. *Immunology* **2012**, *136*, 153−162.

(22) Wang, Y.-D.; Chen, W.-D.; Yu, D.; Forman, B. M.; Huang, W. The G-Protein-Coupled Bile Acid Receptor, GPBAR1 (TGR5), Negatively Regulates Hepatic Inflammatory Response through Antagonizing Nuclear Factor Kappa Light-Chain Enhancer of Activated B Cells (NF-κB) in Mice. *Hepatology* **2011**, *54*, 1421−1432.

(23) Haselow, K.; Bode, J. G.; Wammers, M.; Ehlting, C.; Keitel, V.; Kleinebrecht, L.; Schupp, A.-K.; Häussinger, D.; Graf, D. Bile Acids PKA-Dependently Induce a Switch of the IL-10/IL-12 Ratio and Reduce Proinflammatory Capability of Human Macrophages. *J. Leukocyte Biol.* **2013**, *94*, 1253−1264.
(24) Lewis, N. D.; Patnaude, L. A.; Pelletier, J.; Souza, D. J.; Lukas, S. M.; King, F. J.; Hill, J. D.; Stefanopoulos, D. E.; Ryan, K.; Desai, S.; Skow, D.; Kauschke, S. G.; Broermann, A.; Kuzmich, D.; Harcken, C.; Hickey, E. R.; Modis, L. K. A GPBAR1 (TGR5) Small Molecule Agonist Shows Specific Inhibitory Effects on Myeloid Cell Activation in Vitro and Reduces Experimental Autoimmune Encephalitis (EAE) in Vivo. *PLoS One* **2014**, *9*, e100883.
(25) Bailly, S.; Ferrua, B.; Fay, M.; Gougerot-Pocidalo, M. A. Differential Regulation of IL 6, IL 1 A, IL 1β and TNF-α Production in LPS-Stimulated Human Monocytes: Role of Cyclic AMP. *Cytokine* **1990**, *2*, 205−210.
(26) Foey, A. D.; Field, S.; Ahmed, S.; Jain, A.; Feldmann, M.; Brennan, F. M.; Williams, R. Impact of VIP and cAMP on the Regulation of TNF-α and IL-10 Production: Implications for Rheumatoid Arthritis. *Arthritis Res. Ther.* **2003**, *5*, R317.
(27) Sica, A.; Mantovani, A. Macrophage Plasticity and Polarization: In Vivo Veritas. *J. Clin. Invest.* **2012**, *122*, 787−795.
(28) Faller, B.; Grimm, H. P.; Loeuillet-Ritzler, F.; Arnold, S.; Briand, X. High-Throughput Lipophilicity Measurement with Immobilized Artificial Membranes. *J. Med. Chem.* **2005**, *48*, 2571−2576.
(29) Shultz, M. D. The Thermodynamic Basis for the Use of Lipophilic Efficiency (LipE) in Enthalpic Optimizations. *Bioorg. Med. Chem. Lett.* **2013**, *23*, 5992−6000.
(30) Haveaux, B.; Dekoker, A.; Rens, M.; Sidani, A. R.; Toye, J.; Ghosez, L. α-Chloro Enamines, Reactive Intermediates for Synthesis: 1-Chloro-*N*,*N*,2-trimethylpropenylamine. *Org. Synth.* **1979**, *59*, 26.
(31) Bendall, S. C.; Simonds, E. F.; Qiu, P.; Amir, E. D.; Krutzik, P. O.; Finck, R.; Bruggner, R. V.; Melamed, R.; Trejo, A.; Ornatsky, O. I.; Balderas, R. S.; Plevritis, S. K.; Sachs, K.; Pe'er, D.; Tanner, S. D.; Nolan, G. P. Single-Cell Mass Cytometry of Differential Immune and Drug Responses across a Human Hematopoietic Continuum. *Science* **2011**, *332*, 687−696.
(32) Trunzer, M.; Faller, B.; Zimmerlin, A. Metabolic Soft Spot Identification and Compound Optimization in Early Discovery Phases Using MetaSite and LC-MS/MS Validation. *J. Med. Chem.* **2009**, *52*, 329−335.
(33) Fatouros, D. G.; Karpf, D. M.; Nielsen, F. S.; Mullertz, A. Clinical Studies with Oral Lipid Based Formulations of Poorly Soluble Compounds. *Ther. Clin. Risk Manage.* **2007**, *3*, 591−604.
(34) Elenkov, I. J.; Chrousos, G. P. Stress Hormones, Proinflammatory and Antiinflammatory Cytokines, and Autoimmunity. *Ann. N.Y. Acad. Sci.* **2002**, *966*, 290−303.
(35) Prepared analogously to compound **14**.
(36) Finck, R.; Simonds, E. F.; Jager, A.; Krishnaswamy, S.; Sachs, K.; Fantl, W.; Pe'er, D.; Nolan, G. P.; Bendall, S. C. Normalization of Mass Cytometry Data with Bead Standards. *Cytometry, Part A* **2013**, *83*, 483−494.